A Novel 1×4 Coupler-Multiplexer Permutation Switch for WDM Applications

Tarek A. Ramadan, Robert Scarmozzino, *Member, IEEE,* and Richard M. Osgood, Jr., *Fellow, IEEE*

***Abstract*—A novel 1×4 coupler multiplexer permutation switch (CMPS) is proposed for applications in wavelength-division-multiplexing (WDM) optical networks. The structure of the CMPS integrates the multiplexing and switching functions into a single compact device. It consists of a single-mode/multimode-waveguide grating-assisted, backward-coupler multiplexer followed by a 1×4 digital optical switch (DOS). The specific design uses an InP-based 1×4 CMPS with InGaAsP/InP multiple-quantum-well (MQW) DOS. The calculated values of crosstalk for the coupler multiplexer and the DOS are <-25 dB and -23 dB, respectively, giving an overall crosstalk <-21 dB for channel bandwidths of 10–13 GHz. The device channels are unequally spaced, which reduces unwanted four-wave mixing (FWM), but are fitted to the ITU standard wavelength grid.**

***Index Terms*—Couplers, integrated optics, optical couplers, optical coupling, optical filters, optical switches, waveguide components, wavelength-division multiplexing (WDM).**

I. Introduction

WAVELENGTH-DIVISION multipexing (WDM) is an attractive technique for increasing the aggregate capacity of optical networks by exploiting the wide bandwidth available in optical fibers [1], [2]. The evolution of WDM transmission from simple point-to-point transmission to more complicated multi-user networks with arbitrary physical topologies requires advanced functionality in the optical network nodes (ONN's) such as routing and add/drop functions. However, to preserve the network transparency enabled by optical amplifiers, the functionality burden in the ONN must be shifted to the optical physical-layer, thus stimulating the need for reconfigurable photonic WDM components with high functionality density. At the same time, in transparent optical networks, the accumulation of transmission impairments such as optical fiber dispersion and nonlinearities plays a central role in limiting the performance. For example, the enhancement in the generation of four-wave mixing (FWM) waves due to phase matching near the zero-dispersion wavelength puts a lower limit on the minimum-allowed value of dispersion in dispersion-shifted fibers for WDM systems using equally-spaced channels [2]–[4].

In spite of the obvious advantage of integrating some basic routing and switching functions into a single compact photonic device for WDM applications, the emphasis has been on the design of individual components such as filters, multiplexers, switch arrays, and 2×2 wavelength switching elements [1], [2], [5]. These elements can then be interconnected [6], [7] together or with waveguide-grating routers [8], [9] to perform a specific routing and switching function.

In this paper, a novel 1×4 coupler-multiplexer permutation switch (CMPS), see Fig. 1, which integrates a 1×4 multiplexer followed by a 4×4 switch array, is proposed for applications in WDM optical networks. The CMPS, which is designed for InP-based materials, uses unequally spaced channels, which reduces the FWM-induced crosstalk [2]–[4] The integration of the switching function with the multiplexing function in this CMPS structure enables dynamic changing of the multiplexing pattern. For example, such a capability would allow reconfigurability, at the optical layer level, of the connectivity of a point-to-point transmission system.

This paper is organized as follows. The principle of operation of the CMPS is described in Section II. The design parameters and the simulation results are given in Section III, including the design of the backward-coupler section of the CMPS in Section III-A, and the 1×4 DOS in Section III-B. Finally, Section IV presents concluding comments.

II. Principle of Operation

The central idea of the CMPS is to map the wavelength spectrum of the input WDM channels, carried in a single-mode waveguide, onto the modal spectrum of a multimode waveguide. This mapping allows the spatial separation and switching of these wavelength-assigned modes to result in demultiplexing and permutation of the input channels. The mapping is carried out via a single-mode/multimode waveguide grating-assisted backward coupler.

In the CMPS, each channel of the input signal is phase matched through a grating to the different backward modes of the multimode waveguide such that the power in each channel is coupled to a different mode. The different channels are then separated by a digital optical switch (DOS). The different permutations in the multiplexing pattern are obtained by electrically controlling the effective-index distribution of the DOS output waveguides. The design of CMPS uses InGaAsP/InP multiple-quantum-well (MQW) output waveguides. In this design, the quantum-confined Stark effect [10] (QCSE) is used to allow for a compact, low-driving-voltage device. Regrowth processes are therefore required in the fabrication of this device.

It is possible to examine the feasibility of the basic operation of this device by approximating the waveguide modal fields with sinusoidal functions. This estimate is based on the approximate

Manuscript received June 11, 1999; revised November 16, 1999. This work was supported by DARPA/MURI Grant R5226269101 and a scholarship from the Egyptian Ministry of Higher Education.

The authors are with the Microelectronics Sciences Laboratories, Columbia University, New York, NY 10027 USA.

Publisher Item Identifier S 0733-8724(00)03036-X.

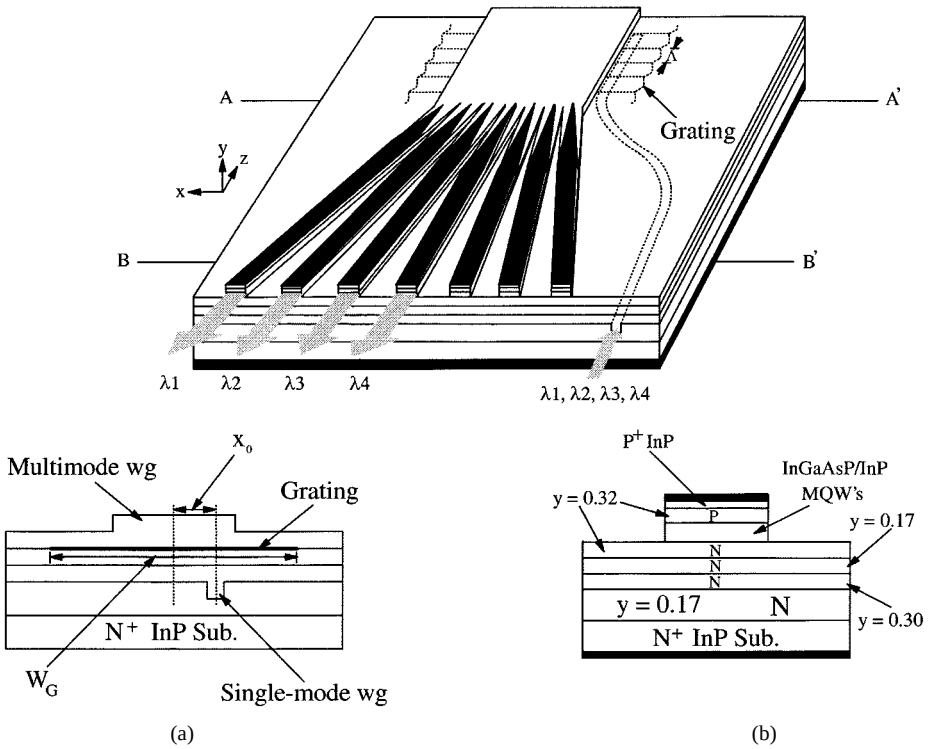

Fig. 1. Schematic layout of the proposed coupler-multiplexer permutation switch: (a) cross section at A–A′ and (b) cross section of an output waveguide at B–B′.

analytical solution obtained for high index confinement [14]. In this case the lateral component, I, of the overlap integral between the normalized modal fields of the single-mode and the multimode waveguides is given by

$$I = \frac{2}{\sqrt{W^{(A)}W^{(B)}}} \int_{-W^{(A)}/2}^{W^{(A)}/2} \cdot \sin\left((k+1)\frac{\pi}{W^{(B)}}\left(x + x_o + \frac{W^{(B)}}{2}\right)\right) \cdot \cos\left(\frac{\pi}{W^{(A)}}x\right) dx. \tag{1}$$

Here $(W^{(A)}, W^{(B)})$ are the single-mode and the multimode waveguide widths, respectively; x_o, is the lateral offset between the centers of the single-mode and the multimode waveguides; and k is the mode index (not the wave vector). In the above equation, it was assumed that complete lateral modal overlap takes place between the single-mode and the multimode waveguides such that

$$|x_o| + \frac{W^{(A)}}{2} \leq \frac{W^{(B)}}{2}. \tag{2}$$

The integration in (1) gives

$$I = \frac{4\sqrt{q}/\pi}{1-(k+1)^2q^2}\cos\left((k+1)q\frac{\pi}{2}\right) \cdot \sin\left((k+1)(p+1)\frac{\pi}{2}\right) \tag{3a}$$

where

$$p = \frac{2x_o}{W^{(B)}}, \quad \text{and} \quad q = \frac{W^{(A)}}{W^{(B)}}. \tag{3b}$$

This result suggests two different design approaches. In the first approach a nonzero value of the normalized offset parameter, p, is used to "excite" all the modes of the multimode waveguide, whereas in the second design approach, only the even-ordered modes are excited by selecting $p = 0$. Because of the advantages of the second approach that are discussed below, this latter approach is examined here. See [15] for more details on the design of the CMPS using the first approach. In order to suppress the modal dependence of the coupling coefficient, the following requirement:

$$q \ll 1/M \tag{4}$$

needs to be satisfied, where $M = k_{\max} + 1$ is the number of multimode-waveguide modes. This requirement means that the single-mode waveguide width should be chosen to be much smaller than the multimode waveguide width.

The bandwidth of the CMPS channels depends almost linearly on the coupling strength between the single-mode and the multimode waveguides [16]. This bandwidth dependence on coupling, which is mainly determined by the nonunifomity in the overlap integral between the modes, puts an upper limit on the number of WDM channels that can be handled by the CMPS. In order to estimate the coupling uniformity into the output modes, a quantity, ρ, defined as

$$\rho \equiv 1 - \min_k |I| / \max_k |I| \tag{5}$$

and limited by $0 \leq \rho \leq 1$, is introduced. Here, $\min_k |I|$, and $\max_k |I|$ refer to the minimum and maximum values of $|I|$ with respect to the mode index, k. Note that the parameter $\rho \to 0$ if the variation in the coupling strength into the set of output modes is small. The calculated minimum values of ρ, for the

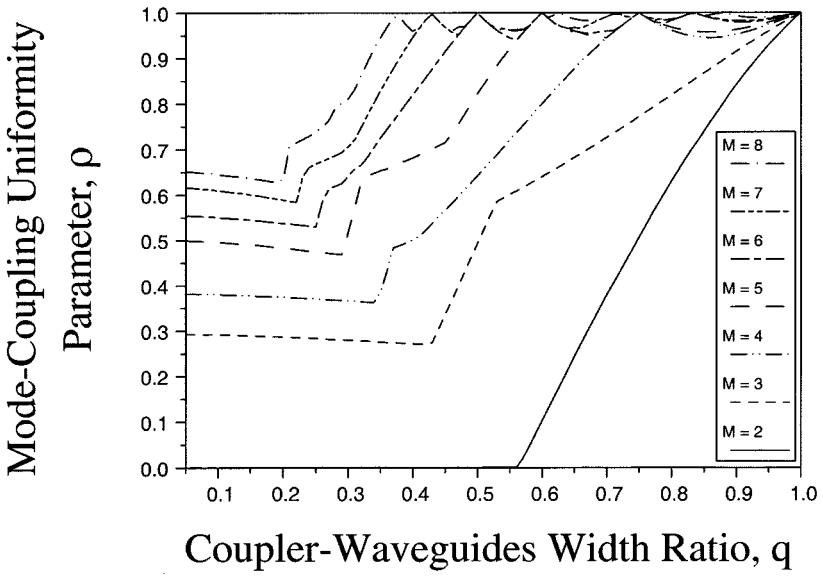

Fig. 2. Mode-coupling uniformity parameter, ρ, as a function of the width ratio, q, in the case of exciting all the modes of the multimode waveguide.

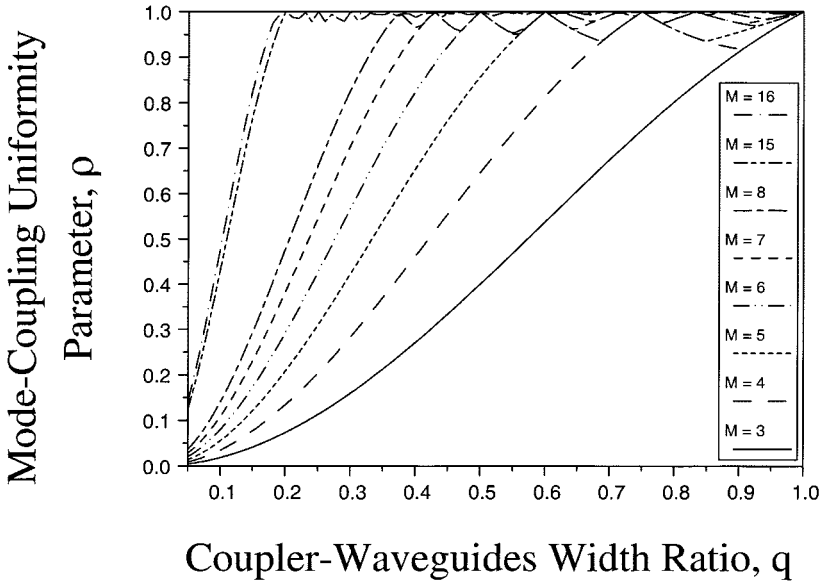

Fig. 3. Mode-coupling uniformity parameter, ρ, as a function of the width ratio, q, in the case of exciting only the even-ordered modes of the multimode waveguide.

case of exciting all the multimode-waveguide modes, are shown in Fig. 2 as a function of the width ratio q for different numbers of output modes, M. In these calculations the minimum value of ρ was taken over the normalized offset parameter, p, for each value of q. The results show that there is a floor on the uniformity of "excitation" of the output modes of the device, which increases with the number of output modes. However, it is found that in the case of exciting only even-ordered modes, there is no floor on this uniformity, as shown in Fig. 3. Thus, in spite of the fact that, in this case, the minimum required number of multimode-waveguide modes is almost twice the number of WDM channels, a larger number of WDM channels can still be used under the same tolerance in bandwidth fluctuations than for the case of exciting all waveguides modes. This is an important motivation for selecting the design approach, described above.

Consider now the feasibility of allocating the CMPS channels to the standard ITU grid. For our device, the channel spacing, between the even-ordered modes [15]

$$\lambda_i - \lambda_{i+2} = \frac{4\Lambda^3 \overline{N}_F^2}{W_{eo}^{(B)2} N_F^{(B)}} \left(\frac{i}{2} + 1\right) \tag{6a}$$

with

$$\overline{N}_F = \frac{N_F^{(A)} + N_F^{(B)}}{2} \tag{6b}$$

is obtained using the phase matching condition,

$$\beta_o^{(A)} + \beta_i^{(B)} = \frac{2\pi}{\Lambda}. \tag{7}$$

Here $(N_F^{(A)}, N_F^{(B)})$ are the core effective indexes of the single-mode and the multimode waveguides, respectively; $W_{eo}^{(B)}$is the effective width of the zero-order mode of the multimode waveguide. The quantities, $(\beta_o^{(A)}, \beta_i^{(B)})$ are the propagation constants of the system-modes that are localized in the single-mode and multimode waveguides, respectively, and Λ is the grating period. The normalized channel spacing, i.e., $i/2+1$, follows the sequence: $1, 2, 3, \ldots, (\lceil M/2 \rceil - 1)$, where $\lceil M/2 \rceil$ is the ceiling value of $M/2$. This sequence is optimal in terms of using the frequency spectrum for unequally spaced channels and requires only six grid units of a standard uniform grid to fit four WDM channels compared to fifteen grid units in the case of exciting all the modes of the multimode waveguide [15]. The nonuniform spectrum of the modes in the step index multimode waveguide give rise to the unequally spaced channels. In brief our results, using this simple analytical analysis, show that exciting only the even modes in the second design approach allows a larger number of channels as well as a more efficient use of wavelength spectrum.

Consider now a more detailed description of the structure, shown in Fig. 1. It consists of a backward coupler followed by a 1×7 DOS with three idle waveguides. The backward coupler couples the forward-propagating mode of a single-mode waveguide with the even-ordered backward-propagating modes of a multimode waveguide, that supports seven guided-modes, through a short-period grating. While both waveguides are single mode in the vertical direction, where coupling takes place, one waveguide is single mode and the other waveguide is multimode in the lateral direction where mode splitting takes place.

A grating is etched in the top structure of the epilayer at the lower boundary of the multimode waveguide in order to couple efficiently the power of each channel in the input signal to a different even-ordered backward propagating mode of the multimode waveguide. This grating period matches the effective index of the single-mode-waveguide mode at wavelength $\lambda_i$to that of the ith even-mode of the multimode waveguide. In the perturbation limit, the crosstalk between the modes can be neglected as they propagate through the multimode waveguide in the backward direction due to the orthogonality of the modes of the ideal-waveguide structure.

The even-ordered modes are then directed to four out of seven different output waveguides of the 1×7 DOS. The permutation of modes among these four waveguides is done by electrically controlling the effective-index distribution in all the output waveguides so that the zero-order mode goes to the waveguide with the highest effective index, the second-order mode goes to the waveguide with the next highest effective index, etc., [11]–[13]. This mode separation is done adiabatically in order to minimize the crosstalk between the different channels. Permutation of effective indexes for the mode-splitter output-waveguides results in 24 permutations in the output-demultiplexing pattern of the 1×4 CMPS.

III. Design and Simulation

Due to the lack of a three-dimensional (3-D) bidirectional beam-propagation method (BPM) simulation tool, the design of the CMPS is carried out in two separate stages. The first stage involves the backward coupler design and the second stage involves the DOS design. Several iterative steps may need to be carried out between the two stages in order to determine device parameters that satisfy the individual design requirements for each stage. The backward-coupler section of the CMPS is polarization sensitive and the design was carried out for E^x polarization.

The InGaAsP–InP material system was used in the design in order to enable monolithic integration of photodetectors, lasers, and optical amplifiers with the device. In addition, the switch requires a MQW structure to provide a refractive-index change via the QCSE in the wavelength range of the erbium-doped fiber amplifier (EDFA) gain.

A. The Backward Coupler Design

1) Background Theory: The design of the backward coupler ensures that the power transferred to the unmatched output modes is negligible compared to the power transferred to the phase-matched output mode. In this case only the backward cross-coupling interaction between the input mode of the single-mode waveguide and the ith mode of the multimode waveguide that is phase matched by a grating of period, Λ, at each channel wavelength, λ_i, needs to be considered.

An important consideration in the design of the backward coupler is the variation of the coupler performance due to modal variations in the coupling coefficient, κ_{oi}, between the single-mode and the ith mode of the multimode waveguide. These changes are determined primarily by the modal dependence of the overlap integral [14], [17]. For a backward coupler of length, L, the ratio, R_{oi}, of the reflected output power of the ith mode, to the incident input power of the single-mode waveguide at the phase-matched wavelength, λ_i, is given by [16]

$$R_{oi} = \tanh^2(\kappa_{oi} L). \tag{8}$$

Thus, unlike the case of forward couplers [16], the saturation behavior of (8) at high values of $\kappa_{oi}L$ suppresses any change in the power transfer ratio, R_{oi}, due to small changes in the coupling coefficient, κ_{oi}, for the different output modes. However, the bandwidth for each wavelength-"tagged" mode is sensitive to variations in κ_{oi}. This bandwidth, $\Delta\lambda_{oi}$, is given by [16]

$$\Delta\lambda_{oi} = \frac{G(\kappa_{oi}L)}{L\dfrac{d}{d\lambda}\left|\beta_o^{(A)} + \beta_i^{(B)}\right|} \tag{9a}$$

with

$$G(\kappa_{oi}L) = 4\sqrt{(\eta L)^2 + (\kappa_{oi}L)^2} \tag{9b}$$

where the quantity, ηL, is the solution of

$$\frac{(\kappa_{oi}L)^2 \sin^2(\eta L)}{(\eta L)^2 + (\kappa_{oi}L)^2 \sin^2(\eta L)} = \frac{1}{2}\tanh^2(\kappa_{oi}L). \tag{9c}$$

At high values of $\kappa_{oi}L$, This expression yields an almost linear dependence of the bandwidth on κ_{oi} [16]. As a result, a constant value of κ_{oi} is necessary for equal coupler-filter bandwidths among the different output modes.

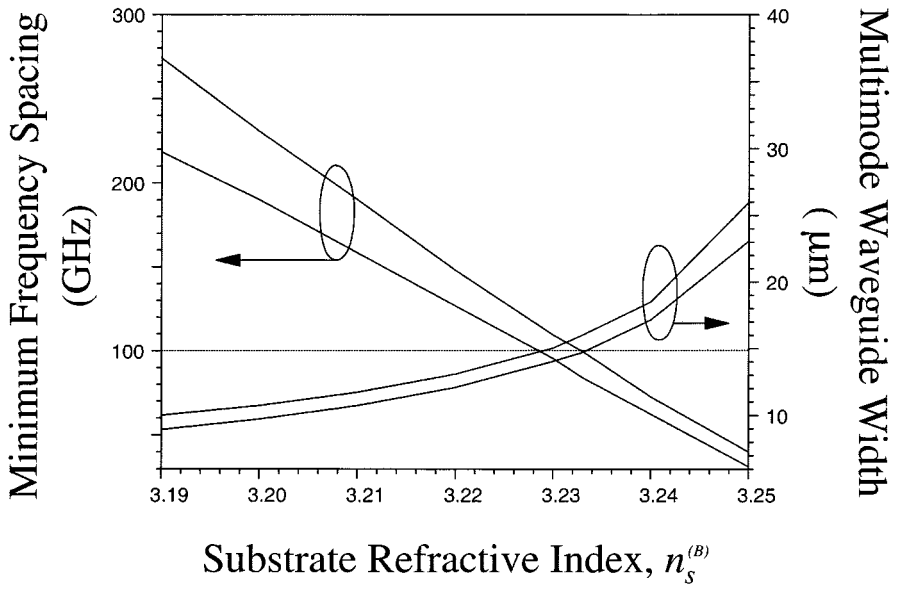

Fig. 4. An upper and lower bounds on the minimum frequency spacing and multimode waveguide width as a function of substrate refractive index $n_s^{(B)}$.

2) Numerical Calculations: The design of the backward coupler of the 1×4 CMPS shown in Fig. 1, is carried out at a design wavelength, $\overline{\lambda} = 1.55\,\mu$m. The core refractive index, $n_f^{(B)} = 3.287$, is chosen in order to match the refractive index of the multimode waveguide to that of the MQW waveguides of the DOS. This index matching is necessary to avoid modal crosstalk at the interface between the backward coupler and the DOS. The lateral width of the multimode waveguide, $W^{(B)}$, is chosen by calculating an upper and lower values, $W_u^{(B)}$and $W_l^{(B)}$, of the waveguide width that support seven guided modes in the lateral direction. Fig. 4 shows the change in $W_u^{(B)}$ and $W_l^{(B)}$as a function of substrate refractive index, $n_s^{(B)}$, for a rib height, $h^{(B)} = 1.1\,\mu$m, and a slab thickness, $t^{(B)} = 0.1\,\mu$m.

Although the multimode waveguide width can take any of the values in Fig. 4 that are bounded by $W_u^{(B)}$ and $W_l^{(B)}$, not all of these values can fit the CMPS channel grid into the standard 0.8 nm (100 GHz) target grid. An additional constraint is therefore required to yield the feasible design parameters. This constraint is obtained by requiring that the unit grid-spacing of the CMPS be equal to 100 GHz, which, in the ideal case, implies that the grating spacing for the subsequent channels is 200 and 300 GHz, respectively. Several 3-D beam propagation method (BPM) calculations of the modal indexes, $N_i^{(B)}$, of the multimode waveguide were carried out at the design wavelength of $1.55\,\mu$m using an iterative technique [18] with a tolerance of 10^{-7}. The values of the minimum and maximum unit grid-spacing, that corresponds to the upper and lower values of the multimode-waveguide width, are shown in Fig. 4, as a function of substrate index, $n_s^{(B)}$. A minimum channel wavelength of 1550.12 nm, as well as, an initial mode-index value, $N_o^{(A)} = n_f^{(A)} = 3.278$, for the single-mode waveguide were used in these calculations. It was found that the replacement of this initial value with the true value of mode index results in a negligible change in the channel frequency spacing. The intersection of the constant 100 GHz line with the unit grid-spacing lines defines the feasible region for the $n_s^{(B)}$ and $W^{(B)}$ design parameters, as shown in Fig. 4. It is clear from that figure that only those values of substrate index, $n_s^{(B)}$, that satisfy, $3.228 \leq n_s^{(B)} \leq 3.233$, can be used in the design to fit the CMPS channels to those of the standard grid. The choice of $n_s^{(B)} = 3.233$ with a multimode-waveguide width of $W^{(B)} = 14.7\mu$m results in channel frequency-spacing of 99.7, 199.4, and 297.9 GHz.

Thus far the CMPS channel frequencies have been calculated based on the modal spectrum of the isolated multimode waveguide. However, the spectrum of the isolated waveguides is perturbed, once the two coupler-waveguides are brought in close proximity to each other. It is, therefore, necessary to optimize the single-mode waveguide parameters, as well as, the vertical separation between the coupler waveguides in order to minimize the perturbation to the multimode waveguide spectrum, which is the main parameter that controls the CMPS channels frequency-spectrum. The selection of the single-mode waveguide parameters: $n_s^{(A)} = n_c^{(A)} = n_s^{(B)}$, $h^{(A)} = 0.7\,\mu$m, $t^{(A)} = 0.1\,\mu$m, and $W^{(A)} = 1.4\,\mu$m with $1.5\,\mu$m vertical separation, results in less than 8.4×10^{-5} change in spectral spacing of the modal indexes, $N_i^{(B)}$. After this optimization, the channel frequency spacing shifts to 99.8, 199.9, and 297.3 GHz. Note that the grating period was left as a "free" parameter that absorbs the changes in the absolute values of the modal indexes in going from isolated-mode calculations to system-mode calculations with the reference wavelength kept at 1550.12 nm. Subsequently the grating period, $\Lambda = 239.572$ nm, was designed to improve the frequency alignment with the standard grid, resulting in less than 3 GHz offset between the CMPS channels and those of the standard grid. In doing this the wavelength dependence of the effective index was accounted for [15]. The calculated CMPS channel frequencies are shown in Table I.

Numerical calculations of the overlap integral of the coupling coefficient [14], [17], were used to compute the grating coupling values. In these calculations the modal field distributions were obtained using a 3-D BPM simulator that employs a finite difference approach [20] and incorporates transparent

TABLE I
RESULTS OF NUMERICAL COMPUTATIONS FOR THE GRATING-ASSISTED BACKWARD-COUPLER

	Mode Number	Wavelength (nm)	Bandwidth (GHz)	CrossTalk (dB)	Offset (nm)
Ch.1	0	1554.901	12.10	- 26.95	0.019
Ch.2	2	1554.099	10.98	- 25.14	0.021
Ch.3	4	1552.505	13.35	- 30.99	0.015
Ch.4	6	1550.138	10.11	- 33.22	0.018

boundary conditions [21]. Fig. 5 shows the calculated values of the minimum CMPS channel bandwidth, the worst case channel crosstalk, and the coupler length as a function of the grating depth, D_g, for more than $\geq 93\%$ power transfer ratio. It is shown that <-25 dB of channel crosstalk can be obtained with <10 GHz bandwidth and a > 8 mm coupler length. The choice of a grating depth, $D_g = 50$ nm, with a coupler length, $L = 8164\,\mu$m, results in a bandwidth that changes from a minimum value of 10.11 GHz for channel 4 to a maximum value of 13.35 GHz for channel 3 with ± 1.6 GHz bandwidth fluctuation. The channel crosstalk values, defined as $10\mathrm{Log}_{10}(\sum_{j\neq i} R_{oj}/R_{oi})$ for the λ_i channel, are better than -25.14 dB, as shown in Table I, where R_{oj} represents the envelope of the oscillatory portion of the power-transfer ratio [14], [16].

B. The Digital Optical Switch Design

1) Background Theory: The multimode waveguide is designed to support seven guided-modes and, hence, the structure of the DOS-branches has seven output waveguides. However, since the WDM channels are coupled only to the even-ordered modes, only four of these output waveguides are used and the others are kept idle. These extra waveguides serve to reduce the DOS crosstalk (see below). In the absence of an external driving voltage, the output waveguides are synchronous, thus forming a "normally on" power splitter operation. However, for the DOS, a distribution of the externally applied voltage to the seven output waveguides is necessary to desynchronize between these output waveguides so that the even-ordered modes go only to four output waveguides. Permutation of the even-ordered wavelength-assigned modes among these four waveguides is done by electrically controlling the effective index distribution so that the zero-order mode goes into the highest-effective-index waveguide, the second-order mode goes into the next highest-effective-index waveguide, etc., [11]–[13]. As the modes propagate from the input waveguide through the output waveguides, they accumulate crosstalk [13] due to the continuous change in local output-waveguide coupling, the mismatch between the local normal modes and the isolated waveguide modes at the output end of the DOS, and the refractive index discontinuity at the starting points of abrupt electrodes.

In order to reduce the refractive-index discontinuity, tapered-width electrodes, see Fig. 1, were introduced to provide adiabatic transitions from the branching points to where the electrodes fully cover the width of the output waveguides. This electrode geometry substantially reduces the crosstalk in the input region and allows for the use of a higher external refractive-index change which can further reduce the crosstalk in the subsequent regions.

The design of a 1×4 DOS is more complicated than that of a 1×2 DOS [13] because of the larger number of interacting local normal modes as well as the dependence of mode conversion on the external index distribution. However, the magnitude of the asynchronicity parameter and the adiabaticity parameter, $\Delta\beta/\gamma\theta \gg 1$, [22]–[24] between individual pairs of output waveguides can guide the design, that ultimately must be carried out with numerical calculations. Here $\Delta\beta$, θ, and γ are the difference in propagation constant of the isolated waveguide modes, the branching angle, and the averaged decay constant for the evanescent fields in the cladding region between the waveguides [24].

A MQW structure was used with electrodes in order to provide external control over the refractive indexes of the output-waveguides. This approach allowed an external voltage-controlled refractive-index change via the QCSE. The QCSE has been shown to enable compact, high speed DOS's, with extremely low driving voltages [25], [26]. Quaternary-compound InGaAsP–InP MQW's were chosen for the MQW structure instead of ternary-compound structures since they provide an extra degree of freedom in which the quantum well width can be chosen for maximum phase modulation and the material composition can be chosen for minimum intensity modulation [27], [28].

The choice of quaternary materials takes advantage of the fact that the spectral change of absorption coefficient drops much faster than the corresponding change in induced refractive index [29] near the exciton edge. The phase modulation is determined by the change, Δn_{eff}, in the waveguide effective index which is related to the refractive index change, Δn, of the MQW medium by, $\Delta n_{\mathrm{eff}} = \Gamma_{\mathrm{MQW}}\Delta n$, where, Γ_{MQW}, is the confinement factor of the unperturbed modal field in the QW layers. For a QCSE device, the value of Δn is proportional to the square of the externally applied electric field, F, and is known from experiments [27] to fall off inversely with the energy detuning, ΔU, from the zero-field exciton resonance. The electro-optic behavior of the QCSE in MQW's can be evaluated with the parameter, $\eta \equiv \Delta n \Delta U/F^2$, which depends only on the quantum-well width and material system [27].

The intensity modulation is determined by the change in the waveguide absorption coefficient, $\alpha_{\mathrm{eff}} = \Gamma_{\mathrm{MQW}}\alpha$, with the applied electric field, where, α, is the absorption coefficient of the MQW medium. Having pure phase modulation is important since the adiabaticity of the DOS structure requires long design lengths in the millimeter range. This requires the operation at a relatively large detuning, ΔU, from the zero-field exciton resonance. At the same time in order to avoid large absorption loss, the device length must be much shorter then the absorption length, $1/\alpha_{\mathrm{eff}}$.

2) Numerical Calculations: The p-i(MQW)-n structure of the DOS rib waveguides is shown in Fig. 1. The $0.51\,\mu$m MQW region consists of 30 periods of undoped

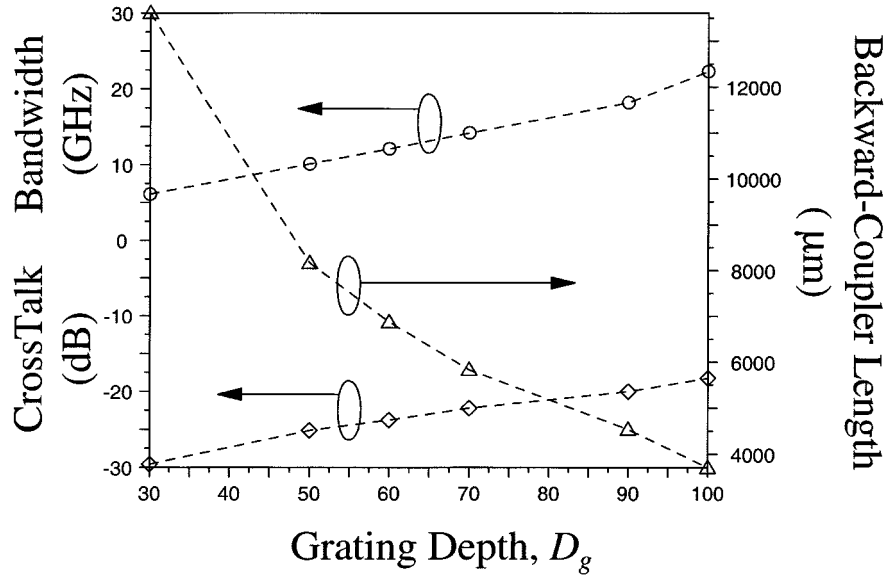

Fig. 5. Minimum bandwidth, maximum crosstalk, and backward-coupler length as a function of grating depth, D_g. The grating is placed at the lower boundary of the multimode waveguide with a grating width of $16\,\mu$m.

$In_{0.64}Ga_{0.36}As_{0.77}P_{0.23}$–InP quantum wells each with an 85 Å barrier and well thickness. Since the thickness of each quantum well period is much smaller then the optical wavelength, the MQW region can be replaced by a single homogeneous layer with an equivalent refractive index [30], [31]

$$n_{\mathrm{MQW}} = \sqrt{\frac{m_W t_W n_W^2 + m_b t_b n_b^2}{m_W t_W + m_b t_b}} \tag{10}$$

for numerical calculations of the E^x mode propagation. Here (m_W, m_b), (t_W, t_b), and (n_W, n_b) are the number, thickness, and refractive index of the quantum well and the barrier regions, respectively. At a wavelength of 1.55 μm, the values of n_W, and n_b used in the calculations [32] are 3.4065 and 3.1631, respectively, which result in the value of $n_{\mathrm{MQW}} \cong 3.287$. The composition of the $In_{0.85}Ga_{0.15}As_{0.32}P_{0.68}$ p-type and n-type confinement layers is chosen to give a homogeneous refractive-index distribution inside the rib-core region. For this distribution, the optical mode is not guided by the thin $0.51\,\mu$m MQW layer. This avoids modal mismatch at the 1×7 DOS branching point.

The confinement factor, Γ_{MQW}, in the QW layers is given by [33]

$$\Gamma_{\mathrm{MQW}} = \Gamma_{eq} \frac{m_w t_w}{m_w t_w + m_b t_b} \tag{11}$$

where $\Gamma_{eq} \cong 0.46$ is the confinement factor of the equivalent $0.51\,\mu$m thickness homogeneous layer and $\Gamma_{\mathrm{MQW}} \cong 0.23$. The value of $\eta \cong 3 \times 10^{-5}$ meV cm^2 kV^{-2} was empirically calculated for similar InGaAsP–InP MQW's [27]. In this design the energy detuning from the zero-field exciton resonance was estimated to be $\Delta U \cong 120$ meV based on the compositional change of the QW layer compared to the previously reported InGaAsP–InP MQW's that have the same QW width [27]. This results in an effective index change of $\Delta n_{\mathrm{eff}} \cong 57.5 \times 10^{-9} F^2$ kV/cm. The small $\cong$2.5 meV change in the value of ΔU due to the different λ's of the WDM channels was neglected.

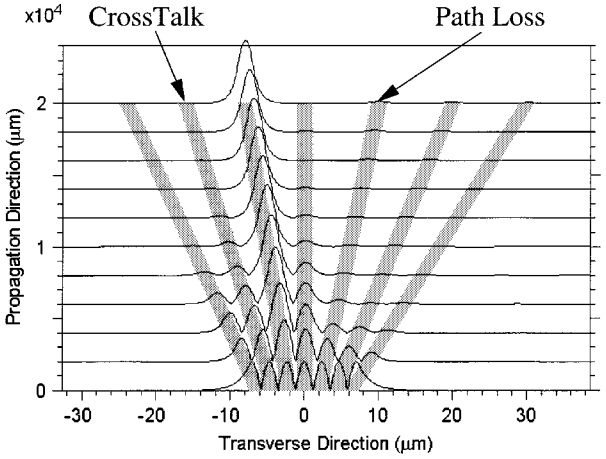

Fig. 6. Simulation of the six-order mode propagation along the DOS. For this permutation the voltage distribution form left to right is 4.40, 8.52, -1.20, 6.73, 7.67, 5.67, and 2.75 V. The three idle waveguides are on the right side of the output waveguides.

Since the actual device is designed for E^x mode operation, a 2-D BPM simulation based on the effective index method [14], [19] was carried out for TM polarization with values of $N_F = 3.2536$, and $N_L = 3.2330$ for the core and cladding refractive indexes, respectively. Calculations of the crosstalk values for these permutations were carried out with different voltage distributions for an assumed overall DOS length of 20 mm with a tapered-electrode-section length of 2 mm, and an edge-to-edge separation of 8 and $10\,\mu$m, for the four output waveguides and the three idle waveguides, respectively. The maximum value of the effective index change, 2.275×10^{-3}, used in these calculations corresponds to an electric field of $\cong$199 kV/cm. This maximum value of electric field is reasonable given that in another MQW structure, with a somewhat wider 94 Å quantum well an experiment showed that the exciton resonance is still resolvable at values of electric field as high as $\cong$220 kV/cm [34]. Our simulation results for an even-mode input are shown

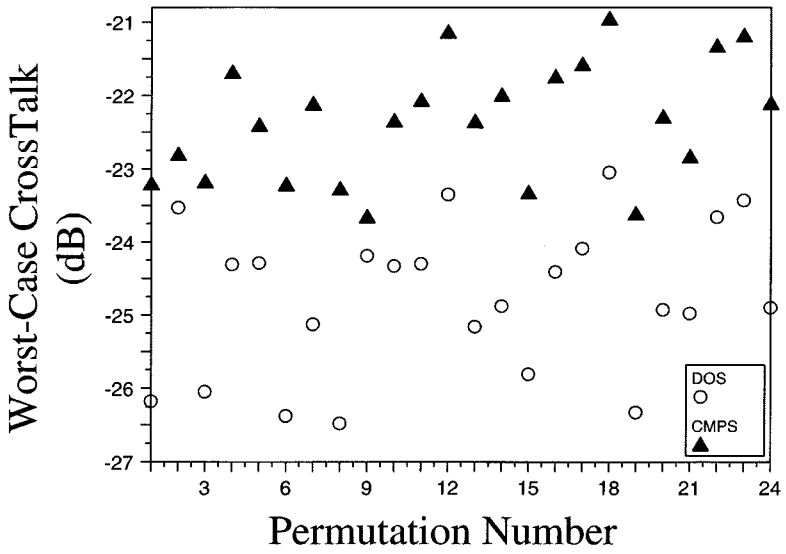

Fig. 7. Results of numerical computations of crosstalk for the 24 permutations of the DOS and the corresponding overall crosstalk of the CMPS.

in Fig. 6, and the overall results for the 24 permutations are summarized in Fig. 7. The results show a worst case crosstalk value of -23.05 dB. Note that unlike the case of mode-power loss to the four output-waveguides, the power loss to the idle waveguides does not result in channel crosstalk; instead, it results only in a relatively small path-loss variation. In our design, the use of idle waveguides allowed the DOS crosstalk to be improved while keeping the variation in path loss to the idle arms <1 dB. This result may be compared to those measured with 4×4 semiconductor switch arrays, no idle elements, where variations in the path loss of $0.5-2.6$ dB have been reported [35], [36].

Another source of path loss variation is the intensity modulation associated with the phase change. In particular, in our proposed design of the CMPS, a reasonable change in path loss might be expected as a result of undesired concomitant intensity modulation. Some insight may be had by comparing our structure with that of a previously reported InGaAsP–InP MQW structure with a 120 Å quantum well width [28], which had the same maximum Stark shift, $\sim F^2 t_w^4$, for an applied field of $\cong$100 kV/cm. For the device of [28], the measured change in absorption due to the change in the bias voltage of that 4 mm-long structure was found to be negligible under comparable energy detuning and Stark shifts. This result suggests a small variation in the path loss in our device. Indeed, the roughness of the etched rib-waveguide core as well as the longer length of the device can add more fabrication constraints in this case.

To estimate the driving voltage required for a given effective index change, Δn_{eff}, the doping concentration on either sides of the i-MQW layer is assumed to be high enough so that the intrinsic layer is fully depleted at zero bias, and the extension of the depletion region outside the intrinsic layer can be neglected. In this case the electric field in the intrinsic layer can be approximated by [37]

$$F = V/d + F_o \tag{12a}$$

with

$$F_o = V_o/d \tag{12b}$$

where d is the intrinsic layer width, and (V, V_o) are the magnitudes of the applied reverse bias voltage and the thermal equilibrium voltage, respectively. The thermal equilibrium voltage, V_o, corresponds to the difference in Fermi-energies on both sides of the intrinsic layer before contact. For example, if $N_A = N_D = 10^{17}$ cm^{-3}, then $V_o \cong 1.2$ V which corresponds to $F_o \cong 24$ kV/cm, and the maximum applied voltage required $\cong$9 V. The value of capacitance, C, of the p-i(MQW)-n structure is $\cong$8.6 pf using the approximation, $C \cong \varepsilon_r \varepsilon_o A/d$, where A is the electrode area, ε_o is the permittivity in free space, and $\varepsilon_r = 12.35$ is the relative static dielectric constant. This corresponds to a $5RC$ switching time of $\cong$2 ns assuming a voltage-source resistance of $R = 50\,\Omega$.

IV. Conclusion

A novel 1×4 coupler-multiplexer permutation switch that integrates the functions of a 1×4 multiplexer followed by a 4×4 switch array is proposed for application in WDM optical networks. In the design approach described here, only the even modes of the multimode waveguide are excited. This approach allows the design of the coupler section of the CMPS with a relatively larger number of WDM channels for a certain tolerance in bandwidth variation. For example, for $q = 0.1$ eight channels can be chosen for a mode-coupling uniformity parameter, $\rho \cong 0.4$. This approach has optimum efficiency in terms of using the frequency spectrum; it is possible to fit nine channels within the $\cong$30 nm bandwidth of the EDFA. This number of channels is the maximum possible number of unequally spaced channels that can fit within the EDFA bandwidth assuming a 0.8 nm grid spacing and $\cong$30 nm bandwidth. In addition, while idle waveguides of the DOS are present, these are important for minimizing the DOS crosstalk within a certain tolerance in path-loss variations. Note that employing a large number of switch branches, N, in a $1 \times N$ DOS is limited by the maximum induced effective-index, $\Delta n_{\text{eff, max}}$. It is straightforward to show using the adiabaticity condition that $N \ll (2\pi/\lambda)(\Delta n_{\text{eff, max}}/\gamma\theta)$. However, many parameters that may improve the performance

of the DOS such as the waveguides profile, the width or height tapering, or the optimum choice of the idle waveguides, have yet to be considered.

Although the coupler section of the CMPS is polarization sensitive, one possible route for accommodating both TE and TM polarizations is to use the excitation symmetry of the device together with diversity reception. For example the output single-mode waveguides of a polarization splitter could symmetrically excite the multimode waveguide, allowing one set of single-mode waveguide parameters to satisfy the phase matching condition for TE modes and the other waveguide parameters to satisfy the same condition for TM modes at the same channel wavelengths. The use of two gratings in series or in parallel with one or two single-mode waveguides may also be possible.

The unequally spaced CMPS channels can be of particular interest in transparent long haul point-to-point optical fiber links that suffers from a FWM nonlinear impairment; see [2]–[4] for a discussion of these points. Other possible applications for the proposed 1×4 CMPS is in local area networks were a closed community of users, requires only a limited number of WDM channels. Finally, larger number of WDM channels can be used by interconnecting several 1×4 CMPS with a $1 \times N$ passive splitter. Another possibility is by using a tree configuration with the "parent" node operating at a coarser grid to provide permutations of wavebands and the "child" nodes operating at a finer grid to provide permutations of the wavelengths within these wavebands.

ACKNOWLEDGMENT

The authors would like to thank Dr. M. Steel for helpful suggestions and careful reading of the manuscript.

REFERENCES

[1] T. E. Stern and K. Bala, *Multiwavelength Optical Networks: A Layered Approach*. Reading, MA: Addison-Wesely, 1999.

[2] G. P. Agrawal, *Fiber-Optic Communication Systems*. New York: Wiley, 1997.

[3] F. Forghieri, R. W. Tkach, A. R. Chraplyvy, and D. Marcuse, "Reduction of four-wave-mixing crosstalk in WDM systems using unequally spaced channels," *IEEE Photon. Technol. Lett.*, vol. 6, pp. 754–756, 1994.

[4] F. Forghieri, R. W. Tkach, and A. R. Chraplyvy, "WDM systems with unequally spaced channels," *J. Lightwave Technol.*, vol. 13, pp. 889–897, 1995.

[5] D. A. Smith, J. E. Baran, J. J. Johnson, and K. W. Cheung, "Integrated-optic acoustically tunable filters for WDM networks," *IEEE J. Select. Areas Commun.*, vol. 8, pp. 1151–1159, 1990.

[6] H. Okayama, T. Kamijoh, and M. Kawahara, "Multiwavelength hiway photonic switches using wavelength-sorting elements-design," *J. Lightwave Technol.*, vol. 15, pp. 607–615, 1997.

[7] J. L. Jackel, M. S. Goodman, J. E. Baran, W. J. Tomlinson, G. Change, M. Z. Iqbal, G. H. Song, K. Bala, C. A. Brackett, D. A. Smith, R. W. Ade, and K. M. Kissa, "Acousto-optic tunable filters (AOTF's) for multiwavelength optical cross-connects: Crosstalk considerations," *J. Lightwave Technol.*, vol. 14, pp. 1056–1066, 1996.

[8] Y. Tachikawa, Y. Inoue, M. Ishii, and T. Nozawa, "Arrayed-waveguide grating multiplexers with loop-back optical paths and its applications," *J. Lightwave Technol.*, vol. 14, pp. 977–984, 1996.

[9] B. Glance, I. P. Kaminow, and R. W. Wilson, "Applications of the integrated waveguide grating router," *J. Lightwave Technol.*, vol. 12, pp. 957–962, 1994.

[10] D. A. B. Miller, D. S. Chemla, and T. C. Damen, "Band-edge electroabsorption in quantum well structures: The quantum-confined Stark effect," *Phys. Rev. Lett.*, vol. 53, pp. 2173–2176, 1984.

[11] B. N. Thruston, E. Kapon, and Y. Silberberg, "Analysis of mode separation in multichannel branching waveguides," *IEEE J. Quantum Electron.*, vol. QE-23, pp. 1245–1255, 1987.

[12] G. J. Veldhuis, J. H. Brends, and P. V. Lambeck, "Design and characterization of a mode-splitting ψ junction," *J. Lightwave Technol.*, vol. 14, pp. 1746–1752, 1996.

[13] H. Okayama and M. Kawahara, "Reduction of voltage-length product for Y-branch digital optical switch," *J. Lightwave Technol.*, vol. 11, pp. 379–387, 1993.

[14] D. Marcuse, *Theory of Dielectric Optical Waveguides*, 2nd ed. New York: Academic, 1991.

[15] T. A. Ramadan, "New optical coupler devices," Ph.D. dissertation, Columbia Univ., New York, 1999.

[16] D. Marcuse, "Bandwidth of forward and backward coupling directional couplers," *J. Lightwave Technol.*, vol. LT-5, pp. 1773–1777, 1987.

[17] ——, "Directional couplers made of nonidentical asymmetric slabs.—Part II: Grating assisted couplers," *J. Lightwave Technol.*, vol. LT-5, pp. 268–273, 1987.

[18] D. Yevick and W. Bardyszewiski, "Correspondence of variational finite-difference (relaxation) and imaginary-distance propagation methods for modal analysis," *Opt. Lett.*, vol. 17, pp. 329–330, 1992.

[19] H. Kogelnik, "Theory of optical waveguides," in *Guided-Wave Optoelectronics*, T. Tamir, Ed. New York: Springer-Verlag, 1988, ch. 2.

[20] R. Scarmozzino and R. M. Osgood Jr., "Comparison of finite-difference and Fourier-transform solutions of parabolic wave equation with emphasis on integrated-optics applications," *J. Opt. Soc. Amer. A*, vol. 8, pp. 724–731, 1991.

[21] G. R. Hadley, "Transparent boundary conditions for beam propagation method," *IEEE J. Quantum Electron.*, vol. 28, pp. 363–370, 1992.

[22] W. K. Burns and A. F. Milton, "Waveguide transitions and junctions," in *Guided Wave Optoelectronics*, T. Tamir, Ed: Springer-Verlag, 1988, ch. 3.

[23] ——, "Mode conversion in planar-dielectric separating waveguides," *IEEE J. Quantum Electron.*, vol. QE-11, pp. 32–39, 1975.

[24] A. F. Milton and W. K. Burns, "Tapered velocity couplers for integrated optics: Design," *Appl. Opt.*, vol. 14, pp. 1207–1212, 1975.

[25] W. Wakita, *Semiconductor Optical Modulators*. New York: Kluwer Academic, 1998.

[26] M. Cada, B. P. Keyworth, J. M. Glinski, A. J. SpringThrope, C. Rolland, and K. O. Hill, "Electro-optic switching in a p-i-n doped multiple quantum well directional coupler," *J. Appl. Phys.*, vol. 69, pp. 1760–1762, 1991.

[27] J. E. Zucker, I. Bar-Joseph, B. I. Miller, U. Koren, and D. S. Chemla, "Quaternary quantum wells for electro-optic intensity and phase modulation at 1.3 and 1.55 μm," *Appl. Phys. Lett.*, vol. 54, pp. 10–12, 1989.

[28] H. K. Tsang, J. B. D. Soole, H. P. LeBlanc, R. Bhat, and M. A. Koza, "Efficient InGaAsP/InP multiple qauntum well waveguide optical phase modulator," *Appl. Phys. Lett.*, vol. 57, pp. 2285–2287, 1990.

[29] J. S. Weiner, D. A. B. Miller, and D. S. Chemla, "Quadratic electro-optic effect due to quantum-confined Stark effect in quantum wells," *Appl. Phys. Lett.*, vol. 50, pp. 842–844, 1987.

[30] M. Born and E. Wolf, *Principles of Optics*, 5th ed: Pergamon, 1975.

[31] R. A. Sammut and I. M. Skinner, "Effective index models for MQW waveguides," *Opt. Commun.*, vol. 76, pp. 213–216, 1990.

[32] S. Adachi, "Optical properties of $In_{1-x}Ga_xAs_yP_{1-y}$ alloys," *Phys. Rev. B*, vol. 39, pp. 12 612–12 621, 1989.

[33] N. Osman, M. Koshiba, and R. Kaji, "A comprehensive analysis of multilayer channel waveguides," *J. Lightwave Technol.*, vol. 12, pp. 821–826, 1994.

[34] D. A. B. Miller, J. S. Weiner, and D. S. Chemla, "Electric-field dependence of linear optical properties in quantum well structures: Waveguide electroabsorption and sum rules," *IEEE J. Quantum Electron.*, vol. QE-22, pp. 1816–1830, 1986.

[35] K. Komatsu, K. Hamamoto, M. Sugimoto, A. Ajisawa, Y. Kohga, and A. Suzuki, "4×4 GaAs/AlGaAs optical matrix switches with uniform device characteristics using alternating $\Delta\beta$ electrooptic guided-wave directional couplers," *J. Lightwave Technol.*, pp. 871–878, 1991.

[36] K. Hamamoto, S. Sugou, K. Komatsu, and M. Kitamura, "Extremely low loss 4×4 GaAs/AlGaAs optical matrix switch," *Electron. Lett.*, pp. 1580–1582, 1993.

[37] P. J. Stevens, M. Whitehead, G. Parry, and K. Woodbridge, "Computer modeling of the electric field dependent absorption spectrum of multiple quantum wee material," *IEEE J. Quantum Electron.*, vol. 24, pp. 2007–2016, 1988.

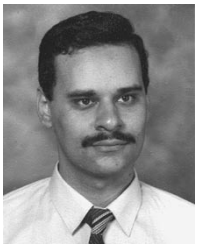

Tarek A. Ramadan was born in Eldakahlia, Egypt. He received the B.S. and M.S. degrees in communications and electronics from Ain-Shams University, Cairo, Egypt, in 1989 and 1994, respectively. His M.S. thesis work was about carrier collection in single quantum-well laser. In 1995, he joined the Electrical Engineering Department, Columbia University, New York, NY, where he is currently working toward his Ph.D. degree in optical communications.

His research at Columbia University involves the design of photonic devices as well as the fabrication and characterization of a lithium niobate crystal-ion-sliced film modulator. From 1989 to 1990, he spent his military-service period at the Military Technical College, and from 1990 to 1995, he worked as a Teaching Assistant and Assistant Lecturer at the Electronics and Electrical-Communications Engineering Department of Ain-Shams University.

Robert Scarmozzino (M'98) received the B.S. and M.S. degrees from the Columbia University School of Engineering and Applied Science, New York, NY, in 1982 and 1983, and the Ph.D. degree from the Columbia University Graduate School of Arts and Sciences in 1987, all in applied physics.

His graduate research was in the area of plasma physics, and primarily consisted of an experimental and theoretical study of collisionless trapped particle instabilities. Subsequent to completing his Ph.D., he joined the Columbia University Microelectronics Sciences Laboratories (MSL) and began research in a variety of laser-induced semiconductor processing techniques, developing novel techniques for etching, deposition, and doping of materials which include semiconductors (Si, GaAs, InP), metals (chiefly Al), and polymers. These techniques have been applied to various device fabrication problems, and several have been transferred to industrial collaborators for potential use in manufacturing. Since 1990, he has been involved in experimental and theoretical work on novel photonic devices. These efforts have led to the realization of several state-of-the-art photonic devices useful for communications and networking applications, and the first demonstration of several new techniques for prototyping photonic integrated circuits. In conjunction with the abovementioned experimental program in integrated optics, he has been active in developing numerical algorithms for the simulation of photonic devices and circuits. In 1994, this work led to the development of BeamPROP, one of the first general purpose software tools for design of photonic devices. Parallel with his research at Columbia University, he cofounded RSoft, Inc. (www.rsoftinc.com), a company specializing in development of CAD and simulation tools for photonic devices and systems. Currently, his primary position is Chief Scientist at RSoft, Inc., but he also continues to work closely with the research group of Prof. R. M. Osgood at the Columbia University Microelectronics Sciences Laboratory.

Dr. Scarmozzino has been a member of the American Physical Society, the Materials Research Society, the Electrochemical Society, the International Society for Optical Engineering, IEEE/LEOS, and the Sigma Xi Society.

Richard M. Osgood, Jr. (SM'82–F'87) received the B.S. degree in engineering from the U.S. Military Academy, the M.S. degree in physics from Ohio State University, Columbus, and the Ph.D. degree in physics at the Massachusetts Institute of Technology (M.I.T.) Cambridge.

He is currently Higgins Professor of Applied Physics and of Electrical Engineering at Columbia University, New York, NY. Prior to this appointment, he served on the scientific staff of M.I.T., Lincoln Laboratory (Solid-State Physics Division), Lexington, MA, the U.S.A.F. Avionics Laboratory, and the U.S.A.F. Materials Laboratory. Throughout his professional career, he has performed research in many areas of optical physics, chemical physics and electrical engineering. His most extensive research has been in the development of new infrared and ultraviolet lasers, the applications of laser-induced chemistry to materials, preparation, and fundamental optical surface physics, and chemistry.

Dr. Osgood is a member of the ACS and MRS and a Fellow of the OSA and the APS. He was also appointed Distinguished Traveling Lecturer of the APS for 19911993 and of IEEECLEOS for 1986. Along with S. Brueck, he organized the first MRS Symposium on Laser Diagnostics and Photochemical Processing. In October of 1983, he was elected to a three-year term as Councillor of the Materials Research Society. In 1990, he was honored with the Japanese Optoelectronic Industry and Technology Development Association (OITDA) Lectureship. In 1991, he received the R. W. Wood Prize from the Optical Society of America. He was formerly the CoDirector of the Columbia Radiation Laboratory and is currently Technical Director. He was also the Director of the Columbia Microelectronics Sciences Laboratories. He has served as a consultant to numerous government and industrial organizations, including the DARPA Defense Sciences Research Council, DOE Basic Energy Sciences Advisory Board, and the Advisory Board for the Los Alamos National Laboratory Chemical Sciences Division. In 1998 he was appointed to the Advisory Board of Brookhaven National Laboratory.